RESEARCH ARTICLE | DECEMBER 02 2025

Sum-frequency-based photon-number-resolving detector for telecom wavelengths

S. Cassina ; A. Pozzoli ; G. Vesco ; M. Lamperti ; M. Marangoni ; A. Allevi

APL Photonics 10, 126104 (2025)
https://doi.org/10.1063/5.0292182

Sum-frequency-based photon-number-resolving detector for telecom wavelengths

Cite as: APL Photon. 10, 126104 (2025); doi: 10.1063/5.0292182
Submitted: 21 July 2025 • Accepted: 11 November 2025 •
Published Online: 2 December 2025

S. Cassina,[1,a] A. Pozzoli,[1] G. Vesco,[2] M. Lamperti,[1] M. Marangoni,[2] and A. Allevi[1]

AFFILIATIONS

[1] Como Lake Institute of Photonics, Dipartimento di Scienza e Alta Tecnologia, Università degli Studi dell'Insubria, Via Valleggio 11, I-22100 Como, Italy
[2] Dipartimento di Fisica, Politecnico di Milano, Polo Territoriale di Lecco, Via G. Previati 1/C, I-23900 Lecco, Italy

[a] **Author to whom correspondence should be addressed:** s.cassina@studenti.uninsubria.it

ABSTRACT

The use of C-band wavelengths in the field of quantum communication has grown significantly, driving the need for versatile detection solutions, especially in the low intensity domain. Among the desirable features for such detectors, photon-number-resolving (PNR) capability is particularly valuable, since it can offer new possibilities for enhancing security of communication protocols. In this paper, we present the implementation of a receiver that combines low-cost PNR detectors with nonlinear optical interactions to achieve sensitivity at telecom wavelengths. In particular, we use this receiver to characterize the Poissonian nature of a femtosecond source at 1.5 μm, produced via white light continuum generation followed by a single-stage amplification process. The obtained results encourage the exploitation of such a detector in more complex schemes.

I. INTRODUCTION

The development of photon-number-resolving (PNR) detectors operating in the infrared spectrum has become a critical priority for advancing quantum communication technologies. Currently, telecommunication infrastructures benefit from the optical fibers optimized for wavelengths around 1550 nm.[1] However, the availability of efficient single-photon and PNR detectors in this spectral region is significantly limited compared to the visible spectral range.

Existing technologies, such as superconducting nanowire single-photon detectors, offer high detection efficiency and low dark counts, but require cryogenic cooling, increasing the operational complexity and cost.[2–5] As an alternative, InGaAs avalanche photodiodes have been widely applied in quantum communication and have seen significant progress in recent years in terms of higher gating frequencies and lower noise performance,[6,7] but their photon-number resolution remains inadequate for advanced quantum protocols.[8,9]

Theoretical and experimental works demonstrated the potential of PNR detectors for applications, such as secure quantum key distribution and quantum state tomography. For instance, in Refs. 10 and 11, theoretical models have highlighted the critical role of photon-number resolution in improving the quantum channel capacity and the secret key generation rate, while the experimental results in Ref. 12 have showcased the feasibility of PNR detectors in quantum optics.

With respect to these applications, some of us have recently demonstrated the suitability of Silicon photomultipliers (SiPMs).[13,14] Indeed, such detectors are compact, robust, low-cost, and have low-power requirements, thus being excellent candidates for quantum communication receivers. In this respect, we have shown that these detectors can be used to reveal nonclassical correlations of mesoscopic twin-beam states of light[15–17] and to perform novel quantum communication protocols.[18] However, their response is limited to the visible and UV ranges.

To overcome these limitations, in this work, we present the implementation of a compact scheme used to extend the operativity of SiPMs to the telecommunication range. In particular, we exploit a sum-frequency generation process to convert light pulses at telecom wavelengths into pulses in the red spectral region, where SiPMs operate. Since we do not have at our disposal a pulsed light

source natively at telecom wavelengths, we produce it by means of cascaded nonlinear optical interactions and use the sum-frequency-based PNR detector to characterize the photon-number distribution of this light source and investigate its deviations from a Poissonian distribution. We characterize the statistical properties of the produced light in terms of the autocorrelation and cross correlation functions proving the potential of our detector in revealing the nature of the measured light.[19]

The obtained results represent a first but fundamental step toward the implementation of a compact receiver operating at telecom wavelengths and characterized by an outstanding PNR capability. In particular, the ultimate goal is to change the direct detection scheme realized in this work to implement a homodyne-like scheme, still based on SiPMs,[13] in which the signal and the low-intensity local oscillator are produced at telecom wavelengths, while their detection is performed in the visible spectral range. The basic scheme includes two SiPMs, but more complex architectures, such as the HYNORE receiver in Ref. 20, are also possible.

II. MATERIALS AND METHODS

The proof-of-principle implementation of a PNR detector sensitive to telecom wavelengths relies on the production of a cascade of nonlinear interactions aimed at preparing, optimizing, and properly tailoring the light source. In view of highlighting the potential of the different steps introduced in the experimental setup, in the following, we present a detailed description of each implemented process.

A. Light generation and amplification at 1550 nm

As shown in Fig. 1, the 190 fs long pulses at 1030 nm of a Yb:KGW amplified laser operated at a repetition rate of 3 kHz are split into two parts by means of a sequence of half-waveplates and polarizing beam splitters (PBSs) in order to finely tune both their polarization and their energy. One portion of light is focused (the focal length of the employed convergent lens is $f = 150$ mm) into a 10 mm thick yttrium aluminum garnet (YAG) plate to produce a white light continuum (WLC) source (see the box WLC in the figure). By pumping the YAG plate with a pulse energy of 1.6 μJ, we obtain the WLC light extending over the entire visible spectral range and spanning up to 1600 nm,[21] as shown in Fig. 2. The spectra were obtained using two different fiber spectrometers: we show as the solid blue line the measurements taken with AvaSpec-ULS2048x64-EVO (Avantes), setting the integration time to 2.4 ms, and as the dotted-dashed red line those acquired with the MiniSpectrometer TG-NIR: C11482GA (Hamamatsu Photonics), setting the integration time to 1 ms. Even though the absolute values depend on the spectral sensitivity curve of the adopted devices, the power spectral density at 1550 nm results much lower than at shorter wavelengths. Since this could represent a limitation for the exploitation of this telecom source in communication protocols, where the signals are typically modulated and can undergo unavoidable losses, we decided to amplify the light by means of a single-pass optical parametric amplifier (OPA).[22] As shown in the box called OPA in Fig. 1, the generated light at 1550 nm is focused by a 100 mm focal length lens and mixed in a β-Barium-Borate (BBO) crystal, cut for type-I phase matching (cut angle = 23.4°, 3 mm long, called BBO1

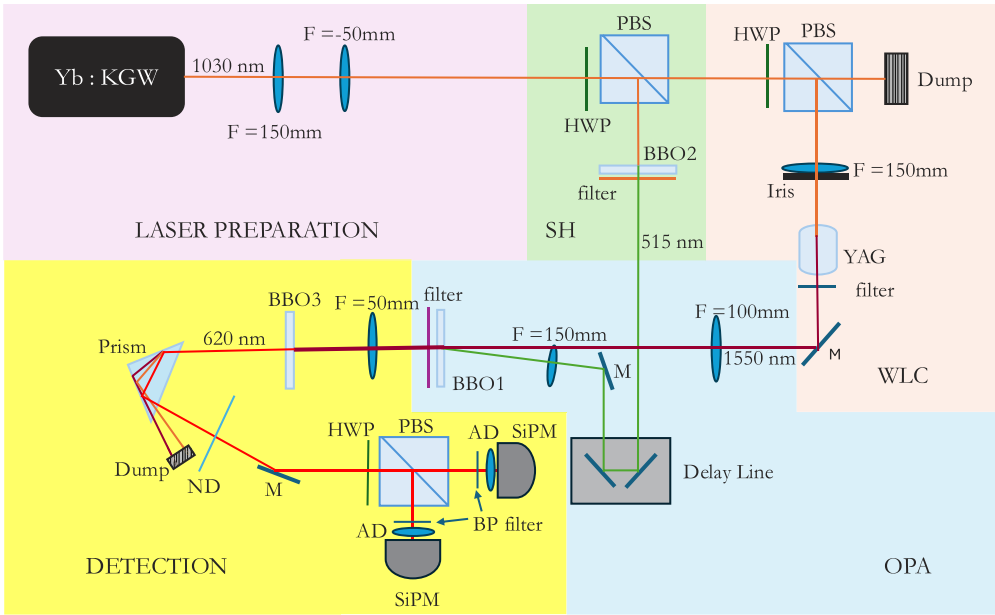

FIG. 1. Sketch of the experimental setup used to produce both the beam at 1550 nm and the one at 620 nm. The colored boxes define the different steps of the setup. WLC: white light continuum; SH: second harmonic; OPA: optical parametric amplifier; F: convergent lens; HWP: half-waveplate; PBS: polarizing beam splitter; BBO1, BBO2, and BBO3: β–Barium-Borate crystals; YAG: yttrium aluminum garnet plate; M: mirror; BP: bandpass filter; ND: neutral density filter; AD: achromatic doublet; and SiPM: Silicon photomultiplier. See the text for details.

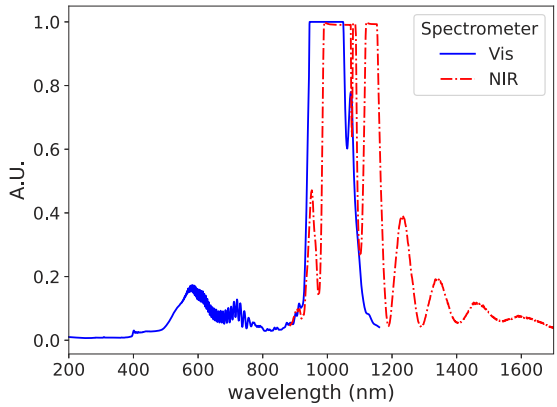

FIG. 2. Solid blue line: spectrum, normalized to the full-scale range, of the WLC in the visible region; dotted-dashed red line: spectrum, normalized to the full-scale range, of the WLC in the infrared region. The fundamental beam at ~1030 nm, whose intensity value exceeds the full-scale range, is also present in the plot.

in the figure), with the second harmonic (SH) (at 515 nm) of the laser by means of a slightly noncollinear interaction geometry to spatially separate the beams after the OPA. The SH is generated by sending one of the infrared portions (with roughly 19 μJ of energy per pulse) into a second BBO crystal cut for type-I phase matching (cut angle = 22.8°, 3 mm long, called BBO2 in the box SH of the figure). The SH is focused by a 150 mm focal-length lens in BBO1 and its temporal delay can be micrometrically varied in order to optimize the temporal overlap with the WLC pulses in the crystal. The spectrum of the amplified light at 1550 nm is shown in Fig. 3(a), along with the spectrum obtained when the SH light does not enter BBO1. The comparison highlights the importance of the amplification stage, which provides a gain of ~10^4 in the region centered at 1550 nm, with a bandwidth of ~50 nm. Both spectra were obtained with the fiber spectrometer sensitive to the infrared spectral range. The spectrum of the amplified light with a bandpass filter centered at 1550 nm is also shown as dashed black curve to highlight the wavelength we are interested in.

B. Sum-frequency generation at 620 nm and detection

As shown in the DETECTION box of Fig. 1, the amplified light at 1550 nm is directed to a further BBO crystal (cut angle = 23.4°, 3 mm long, labeled BBO3 in the figure), where it interacts with the residual infrared light at 1030 nm traveling along the same optical path. This interaction leads to a sum-frequency generation process in a collinear interaction geometry. A typical spectrum of the generated light is shown in Fig. 3(b), which was obtained with the Avantes fiber spectrometer. We note that the conversion efficiency is on the order of few percents because the use of the residual beam at 1030 nm does not allow the optimization of its spot size for the improvement of the upconversion process. Nevertheless, as shown hereafter, the energy of the upconverted beam is sufficient to investigate the nature of the light source at telecom wavelengths and, in particular, to reveal its deviation from Poissonianity. The wavelength of the generated light matches the sensitivity range of the

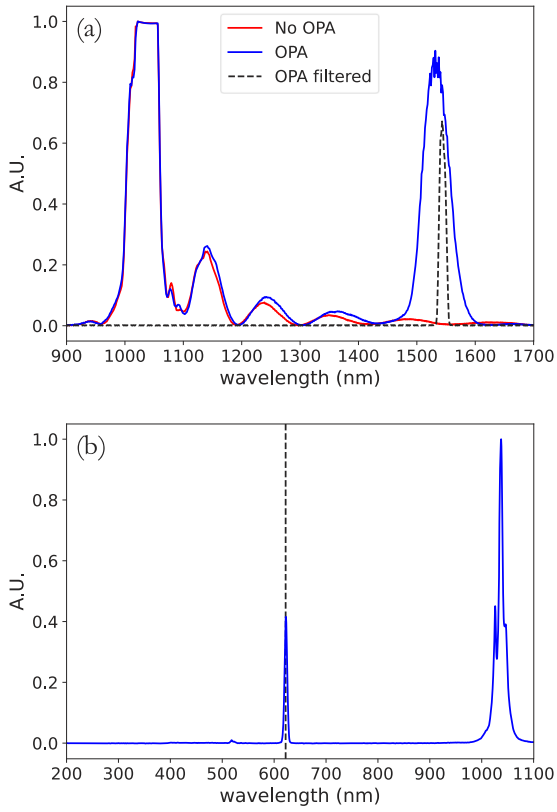

FIG. 3. (a) Spectrum of the white light continuum in the infrared region in the presence (blue curve) and in the absence (red curve) of amplification. The dashed black curve corresponds to the amplified spectrum obtained by using a bandpass filter centered at 1550 nm in front of the spectrometer. (b) Spectrum of the light exiting BBO3, in which the generation of the sum frequency at 620 nm, highlighted by the black dashed line, is clearly evident. Both spectra have been normalized to the full-scale range.

PNR detectors that are embedded in the hybrid receiver described in Ref. 13.

As anticipated in Sec. I, these PNR detectors are SiPMs. They consist of matrices of cells operated in the Geiger–Müller regime with a common output. The model used (mod. MPPC S13360–1350CS, Hamamatsu Photonics) in this proof-of-principle work has 667 squared cells, with a pixel pitch of 50 μm. The quantum efficiency is around 40% in the blue–green region, while it reduces to 25% at 620 nm. However, there are also other models more suitable for the detection in the red spectral range. SiPMs are endowed with an outstanding PNR capability even if they are operated at room temperature, as shown in Fig. 4, which reproduces a typical pulse height spectrum. The two detectors we used to perform the characterization of the generated light are amplified by a fast amplification stage (the amplification gain is equal to 17 dB), and then the output signals are integrated over a 10 ns long gate to reduce the contributions of dark counts and optical crosstalk, which generally affect the SiPMs.[16,23] In particular, by performing a dark measurement of 10^5 samples, we experimentally get a value of about 0.3% of dark counts for both the employed detectors, while the contribution

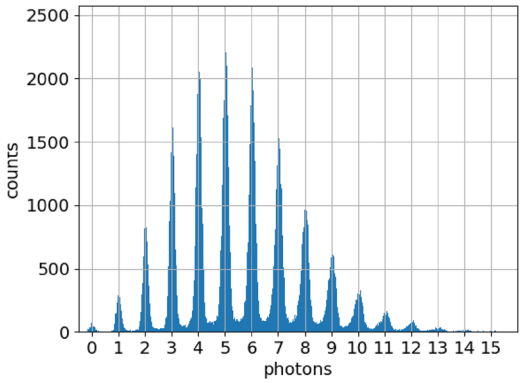

FIG. 4. Typical pulse height spectrum of an amplified SiPM output integrated in a 10 ns gate window, from which the outstanding PNR capability of such a detector is evident. This result is obtained from the 2×10^5 data. The corresponding mean number of photons is $\langle m \rangle = 5.74$.

of crosstalk effect is below 1%. Finally, the analog signals are digitized and acquired. The detection chain implemented so far has a minimum detectable mean number of photons equal to ~0.5, while the maximum detectable mean number of photons is equal to ~15. Further improvements to the detection chain can, in principle, be obtained by replacing the boxcar gated integrators used to integrate the amplified signal outputs with a faster acquisition system. Indeed, these analogical integrators represent the current bottleneck in the detection chain, since they cannot be operated at high repetition rates (>5 kHz). If on the one hand, the rate at which we acquired the measurements in this work, i.e., 3 kHz, does not represent a problem for the recovery time of SiPMs (which is on the order of 5–10 ns, thus setting the maximum acquisition rate to 200 MHz), on the other hand, it is a limitation in view of the practical applications to quantum communication, where faster acquisition systems are typically needed.

Even though the hybrid scheme in Ref. 13 involves an interferometer and a local oscillator, such as in the case of standard optical homodyne detection schemes,[24] the preliminary characterization performed here involves the two SiPMs in a different configuration, which is a direct one. Indeed, since we are mainly interested in investigating the coherence properties of the light generated with the current setup, we used a scheme for the measurements of $g^{(2)}$ autocorrelation and $g^{(1,1)}$ cross correlation functions. As shown in Fig. 1, at the output of BBO3, we place a prism to separate the different wavelengths exiting the crystal, i.e., 620, 1030, and 1550 nm. The red part is then divided at a PBS preceded by a half waveplate to finely tune the balancing between the two output arms of the PBS. Moreover, each output is focused by an achromatic doublet into a multi-mode fiber with 1 mm core diameter and delivered to a SiPM.

C. Theoretical framework

The statistical characterization of the light produced at 620 nm can be achieved by considering either the first moments of the photon-number distribution or the photon-number distribution itself. Indeed, starting from a coherent beam, we expect that the sequence of nonlinear interactions we are realizing does not change its statistical properties.[25,26] In that case, the statistical distribution of the detected photons, to which we have direct access,[27,28] is described by a Poissonian distribution,[29]

$$p(m) = \frac{\langle m \rangle^m}{m!} \exp\left(-\langle m \rangle\right), \tag{1}$$

in which $\langle m \rangle$ is the mean number of detected photons. Moreover, it could be useful to characterize the generated light by considering the autocorrelation and cross correlation (at the PBS) functions, since their value can easily reveal the statistical features of the generated light.[30–32] According to the definition given by Glauber,[33] the second-order autocorrelation function is defined as

$$g^{(2)}(n) = \frac{\langle : n^2 : \rangle}{\langle n \rangle^2} = \frac{\langle n^2 \rangle}{\langle n \rangle^2} - \frac{1}{\langle n \rangle} = 1 + \frac{F(n) - 1}{\langle n \rangle}, \tag{2}$$

where $: \cdot :$ refers to the normal ordering operation and $F(n)$ is the Fano factor $F(n) = \sigma^2(n)/\langle n \rangle$, in which $\sigma^2(n)$ is the variance of the distribution. In the case of Poissonian light, since all the moments of the distribution are equal, $F(n) = 1$. In terms of detected photons, where $\langle m \rangle = \eta \langle n \rangle$, $F(m) = \eta F(n) + (1 - \eta)$, in which η represents the quantum efficiency. Hence, an expression analogous to that in Eq. (2) can be written for detected photons as

$$g^{(2)}(m) = \frac{\langle m^2 \rangle}{\langle m \rangle^2} = g^{(2)}(n) + \frac{1}{\langle m \rangle} = 1 + \frac{F(m) - 1}{\langle m \rangle} + \frac{1}{\langle m \rangle}. \tag{3}$$

In the case of the Poissonian light, we have

$$g^{(2)}(m) = 1 + \frac{1}{\langle m \rangle}. \tag{4}$$

By dividing a Poissonian light at a PBS, it is possible to calculate the shot-by-shot photon-number correlations or the cross correlation function, $g^{(1,1)}$. As shown in Ref. 19, in terms of detected photons, it is defined as

$$g^{(1,1)}(m) = \frac{\langle m_1 m_2 \rangle}{\langle m_1 \rangle \langle m_2 \rangle}, \tag{5}$$

in which m_1 and m_2 are the numbers of detected photons at the two outputs of the PBS. Since in the case of the Poissonian light $\langle m_1 m_2 \rangle = \langle m_1 \rangle \langle m_2 \rangle$, Eq. (5) reduces to

$$g^{(1,1)}(m) = 1. \tag{6}$$

III. RESULTS

Since this work is aimed at demonstrating that the light generated in the mesoscopic intensity regime through the sequence of nonlinear interactions is statistically stable and described by a Poissonian distribution, the first kind of investigation we decided to carry out concerns the statistical properties of the generated light as a function of the power, P, of the fundamental beam (at 1030 nm) used to produce WLC. Indeed, while many characterizations of the coherence of WLC light have been performed in the spectral and spatial frameworks,[34–37] to the best of our knowledge, a systematic analysis in terms of photon-number statistics still lacks.

A. Critical power for WLC generation

In the two panels of Fig. 5, we show the photon-number distributions of detected photons at two different values of P, expressed in terms of critical power: ~4 times the critical power in panel (a) and ~6 times the critical power in panel (b). In general, the critical power, P_{cr}, is defined as the power at which self-action effects may occur as a consequence of the variation of the refractive index of a nonlinear medium because of third-order nonlinear susceptibility.[38] In particular, the critical power is typically associated with the nonlinear phenomena of self-focusing and self-trapping of the light. According to the Marburger's formula,[39] P_{cr} is defined as

$$P_{cr} = \frac{3.72 \cdot \lambda_0^2}{8\pi n_0 n_2}, \tag{7}$$

in which the numerical coefficient, 3.72, is valid for a cylindrically symmetric Gaussian beam. Assuming $\lambda_0 = 1030$ nm, $n_0 = 1.82$, and $n_2 = 6.13 \times 10^{-20}$ m^2/W for the YAG material we used, the critical power happens to be ~1.4 MW, corresponding to an energy of 0.3 μJ per pulse. In both panels, we report as a solid line the Poissonian distribution calculated using the measured mean number of detected photons. The overlap between this distribution and the experimental data is rather poor in panel (a), indicating that the reconstructed distribution deviates from a Poissonian form. In contrast, panel (b) shows a much better agreement, suggesting a closer match to the expected Poissonian behavior. To quantify the discrepancy between theory and experiment, we consider the fidelity parameter, which is defined as $f = \sum_{m=0}^{\bar{m}} \sqrt{p_{th}(m) p_{exp}(m)}$, in which $p_{th}(m)$ and $p_{exp}(m)$ are the theoretical and experimental distributions, respectively, and the sum extends up to the maximum number of detected photons, $\bar{m}$, above which both $p_{th}(m)$ and $p_{exp}(m)$ become negligible. Indeed, we get $f = 0.996\,98$ for panel (a) and $f = 0.999\,94$ for panel (b). To systematically study how the power of the fundamental beam affects the stability of the WLC and thus the Poissonian character of the light at 620 nm, we consider both the autocorrelation function $g^{(2)}$ and the cross correlation function $g^{(1,1)}$ shown in the two panels of Fig. 6, for roughly the same mean value $\langle m \rangle$, obtained by the means of a neutral density filter placed beyond the prism in the DETECTION box.

We note that there is a decreasing trend of $g^{(2)}$ at increasing values of the energy per pulse of the fundamental beam and thus of its power. In particular, $g^{(2)}$ values larger than 1.18, corresponding to the expected value in Eq. (4) for $\langle m \rangle = 5.6$, prove that the values of P close to P_{cr} determine the fluctuations in the number of photons. The same kind of information can be extracted by looking at the behavior of $g^{(1,1)}$, which is equal to 1 only for the values of the energy per pulse larger than 1.58 μJ.

B. Poissonian character of the upconverted field

The study reported in Sec. III A, which examined the photon-number statistics as a function of the 1030 nm pulse power used for WLC generation, identified 1.7 μJ as a safe energy value to prevent deviations from the Poissonian statistics. In this Section, by keeping the fundamental pulse energy for WLC fixed at this value, we studied if the Poissonian character is preserved by varying the mean number of photons of the beam at 620 nm to be sure that the sum-frequency generation process does not introduce any additional noise. For this purpose, a continuously variable neutral density filter, placed beyond the prism, was used to finely adjust its energy per pulse. Figure 7 shows the reconstructed detected-photon distribution at different mean values together with the corresponding Poissonian distributions. High values of fidelity ($f > 0.9999$) prove that the generation of WLC is reasonably stable under the investigated conditions. To better emphasize the Poissonian nature of light, we show in Fig. 8 the values of $g^{(2)}$ and $g^{(1,1)}$ as the functions of the mean number of photons detected in the transmitted arm of the PBS placed in the box DETECTION of Fig. 1. To prove that the obtained values correspond to a reliable and stable condition, in panel (a) of the figure, we also show the results achieved by sending to SiPMs the built-in second-harmonic beam (at 515 nm)

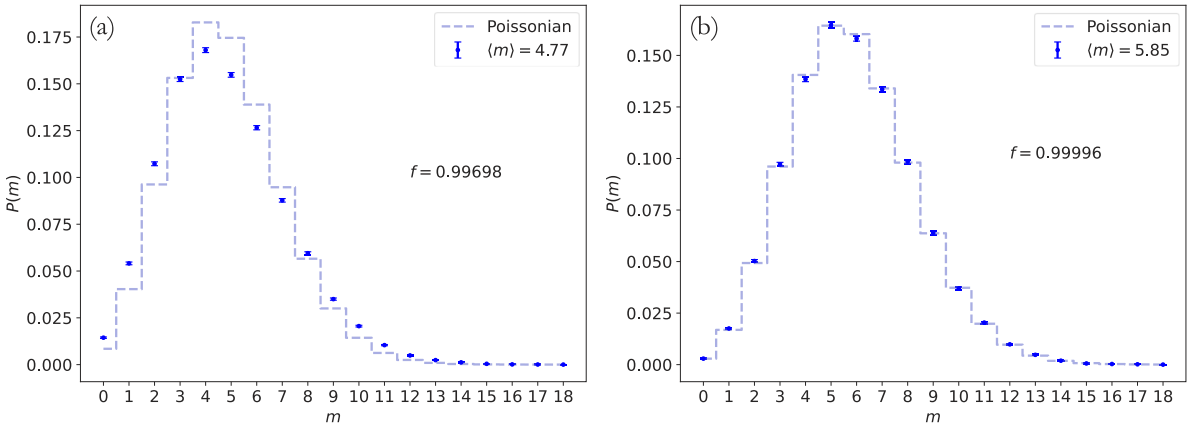

FIG. 5. (a) Reconstructed detected-photon distribution of the upconverted beam at 620 nm when $P \sim 4P_{cr}$ and $\langle m \rangle = 4.77$. (b) Same as in (a) when $P \sim 6P_{cr}$ and $\langle m \rangle = 5.85$. In both panels, dots + error bars correspond to the experimental data, while the dashed line is the theoretical expectation according to the Poisson distribution in Eq. (1). The fidelity values to the Poissonian distributions are $f = 0.996\,98$ in panel (a) and $f = 0.999\,96$ in panel (b). The error applied to each bin is the normalized square root of the bin counts.

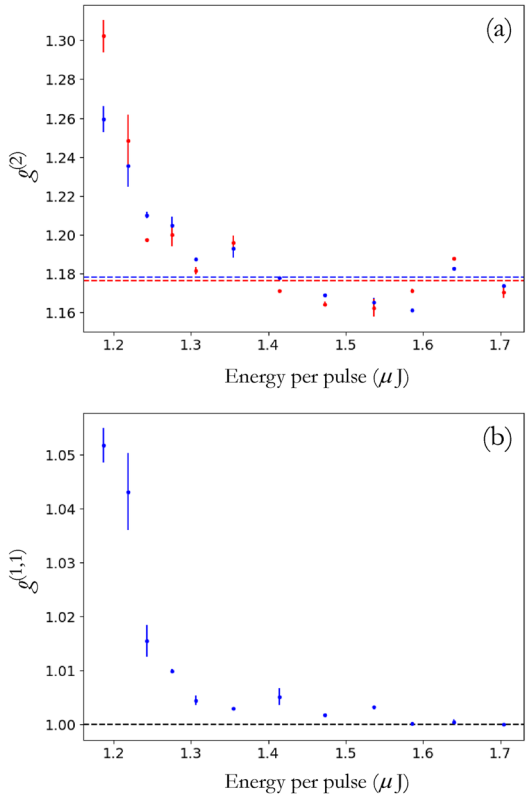

FIG. 6. (a) $g^{(2)}$ autocorrelation function as a function of the energy per pulse of the fundamental beam at 1030 nm. Colored dots + error bars, experimental data corresponding to the two SiPMs and colored dashed lines, expected values in the case of the Poissonian statistics with the mean value equal to $\langle m \rangle = 5.6$. (b) $g^{(1,1)}$ cross correlation function as a function of the energy per pulse of the fundamental beam at 1030 nm. The black dashed line is the expected value in the case of the Poissonian statistics. The experimental results have been obtained by considering four repetitions of the same measurements. The marker with its error bar represents the mean and the associated standard error.

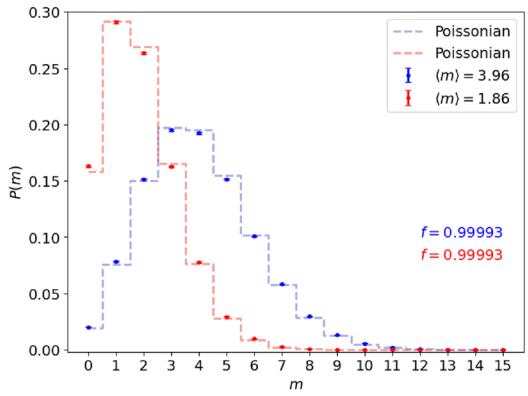

FIG. 7. Reconstructed detected-photon distributions of the upconverted beam at 620 nm for $\langle m \rangle = 3.96$ (blue) and $\langle m \rangle = 1.86$ (red). The dots + error bars correspond to the experimental data, while the colored dashed lines are the corresponding theoretical expectations according to the Poisson distribution in Eq. (1). The fidelity values to the Poissonian distributions are $f = 0.999\,93$ in both cases. The error applied to each bin is the normalized square root of the bin counts.

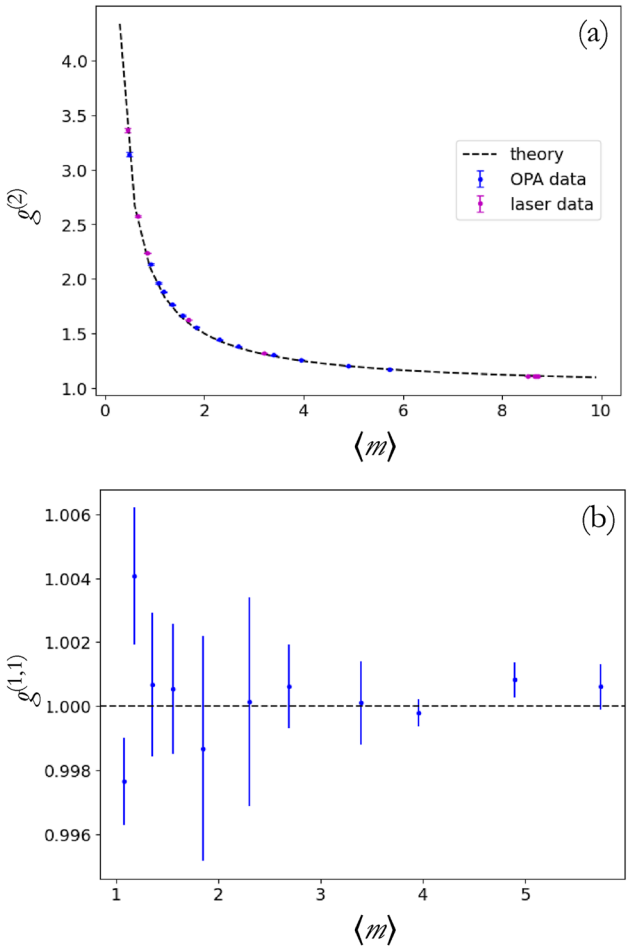

FIG. 8. (a) $g^{(2)}$ autocorrelation function as a function of the mean number of photons detected by the SiPM in the transmitted arm of the PBS in the DETECTION box of Fig. 1. Blue dots + error bars, experimental data corresponding to the beam at 620 nm; magenta dots + error bars, experimental data corresponding to the second harmonic of the laser; and black dashed line, theoretical expectation according to Eq. (4). (b) $g^{(1,1)}$ cross correlation function as a function of the mean number of photons detected by the SiPM in the transmitted arm of the PBS in the box DETECTION. The black dashed line is the theoretical expectation according to Eq. (6). The experimental results have been obtained by considering four repetitions of the same measurements. The marker with its error bar represents the mean and the associated standard error.

of the laser, whose photon-number distribution is described by a Poisson distribution.[13] The variation of the energy of the SH beam was obtained by the means of neutral density filters directly placed at the output of the laser. For the SH and the upconverted beam at 620 nm, the measured values of the autocorrelation function are in good agreement and they are superimposed by the same theoretical curve described by Eq. (4), suggesting therefore that the upconverted beam follows a Poisson distribution. Moreover, in panel (b) of Fig. 8, the calculated values of $g^{(1,1)}$, namely, the cross correlation between the number of photons detected at the two PBS outputs randomly fluctuate around 1, thus indicating that the

statistical distribution is the Poissonian at any mean values of the detected photons.

IV. DISCUSSION

The results obtained as a function of the power of the fundamental beam prove that there is a strict dependence of the statistical properties of the upconverted beam on the stability of the WLC. In fact, appreciable deviations from the Poissonian character of light produced at 620 nm are observed even when the investigated power values are above P_{cr}. This is an interesting result itself as, to the best of our knowledge, the photon-number properties of the WLC are not a deep-investigated subject. Further investigations on this topic could be addressed using different nonlinear materials, such as potassium gadolinium tungstate (KGW), which can produce a WLC more extended in the infrared spectral range.[40] In particular, it would be interesting to study the stability of the WLC as a function of the power and compare the results with those obtained with the YAG plate. In addition, it might be useful to analyze the dependence of the statistical properties on the beam waist size and on the beam waist position with respect to the input face of the nonlinear crystal, as these represent two additional critical parameters alongside power.

Moreover, the study of the photon-number distribution by varying the mean number of photons proves that the source produced at 620 nm does not introduce any noise, thus fully respecting the Poissonian character at any intensity values that can be explored by the means of SiPMs. This supports the fact that the chosen value of the power of the fundamental beam is sufficient to guarantee the robustness of the source. Even the comparison with a native Poissonian light proves this statement. This represents an important step toward the further development of the receiver. One of the improvements is the realization of a sum-frequency process that uses two different paths for the light at 1030 nm and that at 1550 nm in order to suitably modulate[41] the beam only at the telecom wavelengths. Thus, the investigation carried out in this work represents a crucial point to be fixed in view of the application of the detection system in communication protocols. In particular, the PNR capability of the detector could be useful to improve the quantum channel capacity and the secret key generation rate in continuous variable quantum key distribution, thus making it a valid alternative to standard detection systems involving single-photon detectors,[2,6–8] both cryogenic or not, also at ultra-long distances.[5,42]

V. CONCLUSIONS

In this work, we have presented the proof-of-principle implementation of a receiver based on SiPMs and nonlinear optical interactions. The detector has been exploited to characterize a femtosecond laser source at 1550 nm produced by the means of a WLC process followed by an OPA. The detector has enabled the investigation of the statistical nature of the WLC light as a function of the power of the fundamental beam at 1030 nm. The achievement of a stable condition has been investigated as a function of the mean number of photons detected at 620 nm. The use of two SiPMs has allowed us to perform all these studies both in terms of the autocorrelation and cross correlation functions. The agreement of the results with the theoretical expectations opens new perspectives in the use of such a detector in more complex schemes suitable for quantum communication applications. For instance, the PNR capability of our detector would enable discrimination of multi-photon events and improve the overall reliability of communication links in architectures that employ independent heralded single-photon sources.[42] In view of these applications, the detection apparatus will involve a Mach–Zehnder interferometer,[13] in which the signal state will be mixed with a low-intensity local oscillator that will be converted as the signal from telecom wavelengths to visible ones.

ACKNOWLEDGMENTS

M.L. and A.A. acknowledge support from Grant No. PNRR D.D.M.M. 737/2021 and S.C. from PNRR D.D.M.M. 351/2022. Scientific support from the CRIETT center of University of Insubria (Instrument Code: MAC27) is greatly acknowledged. The authors acknowledge Dr. Pietro Anzini (University of Insubria) for the loan of the fiber spectrometer MiniSpectrometer TG-NIR: C11482GA.

AUTHOR DECLARATIONS

Conflict of Interest

The authors have no conflicts to disclose.

Author Contributions

S. Cassina: Data curation (equal); Formal analysis (equal); Methodology (equal); Writing – original draft (equal); Writing – review & editing (equal). **A. Pozzoli**: Data curation (equal); Formal analysis (equal); Writing – review & editing (equal). **G. Vesco**: Data curation (equal); Methodology (equal); Writing – review & editing (equal). **M. Lamperti**: Conceptualization (equal); Software (equal); Writing – review & editing (equal). **M. Marangoni**: Conceptualization (equal); Software (equal); Writing – review & editing (equal). **A. Allevi**: Conceptualization (equal); Data curation (equal); Methodology (equal); Writing – original draft (equal); Writing – review & editing (equal).

DATA AVAILABILITY

The data that support the findings of this study are available from the corresponding author upon reasonable request.

REFERENCES

[1] G. Cariolaro, *Quantum Communications* (Springer International Publishing, 2015).
[2] X. Zhang *et al.*, "NbN superconducting nanowire single-photon detector with 90.5% saturated system detection efficiency and 14.7 ps system jitter at 1550 nm wavelength," IEEE J. Sel. Top. Quantum Electron. **28**, 3803708 (2022).
[3] E. Schmidt, E. Reutter, M. Schwartz, H. Vural, K. Ilin, M. Jetter, P. Michler, and M. Siegel, "Characterization of a photon-number resolving SNSPD using Poissonian and sub-poissonian light," IEEE Trans. Appl. Supercond. **29**, 2201305 (2019).
[4] T. Gerrits, N. Thomas-Peter, J. C. Gates, A. E. Lita, B. J. Metcalf, B. Calkins, N. A. Tomlin, A. E. Fox, A. L. Linares, J. B. Spring, N. K. Langford, R. P. Mirin, P. G. R. Smith, I. A. Walmsley, and S. W. Nam, "On-chip, photon-number-resolving, telecommunication-band detectors for scalable photonic information processing," Phys. Rev. A **84**, 060301(R) (2011).

[5]S. Wang, Z.-Q. Yin, D.-Y. He, W. Chen, R.-Q. Wang, P. Ye, Y. Zhou, G.-J. Fan-Yuan, F.-X. Wang, W. Chen, Y.-G. Zhu, P. V. Morozov, A. V. Divochiy, Z. Zhou, G.-C. Guo, and Z.-F. Han, "Twin-field quantum key distribution over 830-km fibre," Nat. Photonics **16**, 154–161 (2022).
[6]J.-L. Chen, D.-Y. He, S. Wang, Y.-L. Shi, J.-Q. Geng, Z.-Q. Yin, W. Chen, G.-J. Fan-Yuan, G.-C. Guo, and Z.-F. Han, "Low noise InGaAs/InP single-photon detector with DC to 1 GHz tunable gate frequency," Photonics Res. **12**, 3027–3032 (2024).
[7]Z. Yan, T. Shi, Y. Fan, L. Zhou, and Z. Yuan, "Compact InGaAs/InP single-photon detector module with ultra-narrowband interference circuits," Adv. Devices Instrum. **4**, 0029 (2023).
[8]J. C. Campbell, "Recent advances in telecommunications avalanche photodiodes," J. Lightwave Technol. **25**, 109–121 (2007).
[9]M. T. DiMario and F. E. Becerra, "Robust measurement for the discrimination of binary coherent states," Phys. Rev. Lett. **121**, 023603 (2018).
[10]M. Cattaneo, M. G. A. Paris, and S. Olivares, "Hybrid quantum key distribution using coherent states and photon-number-resolving detectors," Phys. Rev. A **98**, 012333 (2018).
[11]M. N. Notarnicola and S. Olivares, "Employing weak-field homodyne detection for optical communications," IEEE J. Sel. Areas Commun. **43**, 1524–1535 (2025).
[12]M. T. DiMario, L. Kunz, K. Banaszek, and F. E. Becerra, "Optimized communication strategies with binary coherent states over phase noise channels," npj Quantum Inf. **5**, 65 (2019).
[13]A. Sanvito, S. Cassina, M. Lamperti, M. N. Notarnicola, S. Olivares, and A. Allevi, "Assessing a binary quantum channel exploiting a silicon photomultiplier based hybrid receiver," Opt. Express **32**, 39846–39859 (2024).
[14]S. Cassina, M. N. Notarnicola, S. Olivares, and A. Allevi, "On the application of a silicon photomultiplier-based receiver for binary phase-shift-keying protocols," Phys. Lett. A **541**, 130403 (2025).
[15]G. Chesi, L. Malinverno, A. Allevi, R. Santoro, M. Caccia, and M. Bondani, "Measuring nonclassicality with silicon photomultipliers," Opt. Lett. **44**, 1371–1374 (2019).
[16]S. Cassina, A. Allevi, V. Mascagna, M. Prest, E. Vallazza, and M. Bondani, "Exploiting the wide dynamic range of silicon photomultipliers for quantum optics applications," EPJ Quantum Technol. **8**, 4 (2021).
[17]A. Pozzoli, M. Lamperti, M. Clerici, M. Bondani, and A. Allevi, "Optimal generation of mesoscopic twin-beam states by means of a natively femtosecond laser system," APL Photonics **10**, 036116 (2025).
[18]L. Razzoli, A. Pozzoli, and A. Allevi, "Hybrid discrimination strategy in quantum communication based on photon-number-resolving detectors and mesoscopic twin-beam states," Quantum Sci. Technol. **10**, 045036 (2025).
[19]A. Allevi, S. Olivares, and M. Bondani, "Measuring high-order photon-number correlations in experiments with multimode pulsed quantum states," Phys. Rev. A **85**, 063835 (2012).
[20]M. N. Notarnicola, M. G. A. Paris, and S. Olivares, "Hybrid near-optimum binary receiver with realistic photon-number-resolving detectors," J. Opt. Soc. Am. B **40**, 705 (2023).
[21]A. Villa, A. M. Ross, R. Gotti, M. Lamperti, F. Scotognella, G. Cerullo, and M. Marangoni, "Broadly tunable mid-infrared femtosecond pulses directly generated by an optical parametric amplifier," OSA Contin. **4**, 2837–2844 (2021).
[22]F. Gucci, A. Baserga, L. Moretti, D. Gatti, M. Corti, C. Manzoni, G. Cerullo, M. Marangoni, and G. Vesco, "Spectral broadening of μJ-level pulses around 8 μm in a Germanium-based multi-pass scheme," Opt. Express **32**, 48599–48609 (2024).
[23]G. Chesi, L. Malinverno, A. Allevi, R. Santoro, M. Caccia, A. Martemiyanov, and M. Bondani, "Optimizing silicon photomultipliers for quantum optics," Sci. Rep. **9**, 7433 (2019).
[24]A. I. Lvovsky and M. G. Raymer, "Continuous-variable optical quantum-state tomography," Rev. Mod. Phys. **81**, 299 (2009).
[25]J. L. Debethune, "Quantum correlation functions for radiation fields with stationary independent modes," Nuovo Cim. **12**, 101–117 (1972).
[26]P. Chmela, Z. Ficek, and S. Kielich, "Classical theory of non-degenerate sum-frequency generation by incoherent nonlinear optical mixing of coherent and chaotic radiations," Czech J. Phys. **39**, 509–528 (1989).
[27]A. Allevi and M. Bondani, "Nonlinear and quantum optical properties and applications of intense twin-beams," Adv. At., Mol., Opt. Phys. **66**, 49–110 (2017).
[28]J. Peřina, Jr., O. Haderka, A. Allevi, and M. Bondani, "Absolute calibration of photon-number-resolving detectors with an analog output using twin beams," Appl. Phys. Lett. **104**, 041113 (2014).
[29]L. Mandel and E. Wolf, *Optical Coherence and Quantum Optics* (Cambridge University Press, Cambridge, UK, 1995).
[30]W. Vogel, "Nonclassical correlation properties of radiation fields," Phys. Rev. Lett. **100**, 013605 (2008).
[31]M. Avenhaus, K. Laiho, M. V. Chekhova, and C. Silberhorn, "Accessing higher order correlations in quantum optical states by time multiplexing," Phys. Rev. Lett. **104**, 063602 (2010).
[32]J. Peřina, Jr., "Coherence and dimensionality of intense spatiospectral twin beams," Phys. Rev. A **92**, 013833 (2015).
[33]R. J. Glauber, "The quantum theory of optical coherence," Phys. Rev. **130**, 2529 (1963).
[34]D. Majus and A. Dubietis, "Statistical properties of ultrafast supercontinuum generated by femtosecond Gaussian and Bessel beams: A comparative study," J. Opt. Soc. Am. B **30**, 994–999 (2013).
[35]A. van de Walle, M. Hanna, F. Guichard, Y. Zaouter, A. Thai, N. Forget, and P. Georges, "Spectral and spatial full-bandwidth correlation analysis of bulk-generated supercontinuum in the mid-infrared," Opt. Lett. **40**, 673–675 (2015).
[36]A. Dubietis, G. Tamošauskas, R. Šuminas, V. Jukna, and A. Couairon, "Ultrafast supercontinuum generation in bulk condensed media," Lith. J. Phys. **57**, 113–157 (2017).
[37]A. Halder, V. Jukna, M. Koivurova, A. Dubietis, and J. Turunen, "Coherence of bulk-generated supercontinuum," Photonics Res. **7**, 1345–1353 (2019).
[38]R. W. Boyd, *Nonlinear Optics* (Elsevier, 2008).
[39]J. H. Marburger, "Self-focusing: Theory," Prog. Quantum Electron. **4**, 35–110 (1975).
[40]V. Marčiulionytė, J. Banys, J. Vengelis, R. Grigutis, G. Tamošauskas, and A. Dubietis, "Low-threshold supercontinuum generation in a homogeneous bulk material at 76 MHz pulse repetition rate," Opt. Lett. **48**, 4609–4612 (2023).
[41]F. Grosshans, G. Van Assche, J. Wenger, R. Brouri, N. J. Cerf, and P. Grangier, "Quantum key distribution using Gaussian-modulated coherent states," Nature **421**, 238–241 (2003).
[42]X.-H. Zhan, Z.-Q. Zhong, J.-Y. Ma, S. Wang, Z.-Q. Yin, W. Chen, D.-Y. He, G.-C. Guo, and Z.-F. Han, "Experimental demonstration of long distance quantum communication with independent heralded single photon sources," npj Quantum Inf. **11**, 73 (2025).